Triply differential (e,2e) studies of phenol

Journal Item

Triply differential (e,2e) studies of phenol

Cite as: J. Chem. Phys. **141**, 124307 (2014); https://doi.org/10.1063/1.4896072
Submitted: 07 August 2014 . Accepted: 08 September 2014 . Published Online: 24 September 2014

G. B. da Silva, R. F. C. Neves, L. Chiari, D. B. Jones, E. Ali, D. H. Madison, C. G. Ning, K. L. Nixon, M. C. A. Lopes, and M. J. Brunger

Triply differential (e,2e) studies of phenol

G. B. da Silva,[1,2] R. F. C. Neves,[1,3,4] L. Chiari,[1,a)] D. B. Jones,[1] E. Ali,[5] D. H. Madison,[5] C. G. Ning,[6] K. L. Nixon,[4] M. C. A. Lopes,[4] and M. J. Brunger[1,7,b)]
[1]*School of Chemical and Physical Sciences, Flinders University, GPO Box 2100, Adelaide, South Australia 5001, Australia*
[2]*Universidade Federal de Mato Grosso, Barra do Garças, MT 78600-000, Brazil*
[3]*Instituto Federal do Sul de Minas Gerais, Câmpus Poços de Caldas, MG, Brazil*
[4]*Departamento de Física, UFJF, Juiz de Fora, 36036-330, MG, Brazil*
[5]*Department of Physics, Missouri University of Science and Technology, Rolla, Missouri 65409, USA*
[6]*Department of Physics, State Key Laboratory of Low-Dimensional Quantum Physics, Tsinghua University, Beijing 100084, China*
[7]*Institute of Mathematical Sciences, University of Malaya, 50603 Kuala Lumpur, Malaysia*

(Received 7 August 2014; accepted 8 September 2014; published online 24 September 2014)

We have measured (e,2e) triple differential cross sections (TDCS) for the electron-impact ionisation of phenol with coplanar asymmetrical kinematics for an incident electron energy of 250 eV. Experimental measurements of the angular distribution of the slow outgoing electrons at 20 eV are obtained when the incident electron scatters through angles of −5°, −10°, and −15°, respectively. The TDCS data are compared with calculations performed within the molecular 3-body distorted wave model. In this case, a mixed level of agreement, that was dependent on the kinematical condition being probed, was observed between the theoretical and experimental results in the binary peak region. The experimental intensity of the recoil features under all kinematical conditions was relatively small, but was still largely underestimated by the theoretical calculations. © *2014 AIP Publishing LLC*. [http://dx.doi.org/10.1063/1.4896072]

I. INTRODUCTION

Electron-impact ionisation of atoms and molecules is a fundamental process which is relevant to understand and interpret a wide range of scientific phenomenon and technological applications, including plasma physics,[1] planetary atmospheres,[2] and radiation-interactions with living tissue.[3] With the exception of the simpler atomic species,[4] the mechanisms of how low- and intermediate-energy electrons ionise atoms and molecules are still not particularly well understood. Measurements of triple differential cross sections (TDCS) for electron impact ionisation of atoms and molecules, using so-called (e,2e) experiments, represent an ideal testing ground to assess the reliability and limitations of theoretical models aimed at describing the ionisation process. In (e,2e) experiments, an electron with well-defined energy and momentum ionises an atomic or molecular target, with the two outgoing electrons being detected in time coincidence. As both the energies and momenta of the two-outgoing electrons are determined in the experiment, a kinematically complete picture of the ionisation process is obtained.

Recently, the dynamical (e,2e) approach has received renewed attention through its ability to provide essential molecular scattering data that can assist in understanding and quantifying the effects of ionisation-related radiation damage in living tissues.[5,6] It is now well established that a single high-energy ionising particle can liberate large numbers of low-energy secondary electrons that deposit energy as they thermalise in living tissue. In addition to the primary ionising particles (e.g., photons, protons, positrons), these low-energy electrons may also induce cell damage.[7] Thus, the way in which those electrons ionise atoms and molecules is, while being only one component in a complex picture, essential to understand the radiation-induced damage. The fundamental atomic and molecular physics scattering data, obtained from experiment and theory, is now being exploited to develop sophisticated charged-particle simulation codes that will be essential for describing charged particle transport in the biological media.[8]

The successful approach of employing electron scattering data in characterising radiation-induced damage within biological systems can be equally applied to other physical systems. One such system is the treatment of biomass by atmospheric pressure plasmas.[9–12] Here, free-electrons or radicals produced within plasmas have the potential to overcome the natural resilience of biomass to degradation.[13,14] In particular, lignocellulose may be broken down by electron impact to fermentable sugars, to intensify the enzymatic hydrolysis process, and improve bio-ethanol yields. However, to exploit charged-particle and plasma simulation of novel applications we require new and diverse sets of complete cross sections from prototypical molecules relevant to the application. Phenol (C_6H_5OH, see Fig. 1), has been identified as a potential target of electron-induced breakdown of lignin (a phenolic based species). Specifically, phenol is known to readily photo-dissociate through conical intersections.[15,16] This has prompted recent theoretical and experimental investigations into electron-driven interactions with phenol[17,18] (and references therein) as a prototypical subunit of lignin.

a)Present Address: Department of Physics, Tokyo University of Science, 1-3 Kagurazaka, Shinjuku-ku, Tokyo 162-8601, Japan.
b)Electronic mail: Michael.Brunger@flinders.edu.au

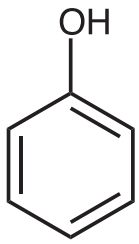

FIG. 1. A schematic representation for the structure of phenol.

Electron-impact ionisation is also a potential strategy for biomass degradation, and makes the investigation into the dynamics of electron-impact ionisation of phenol relevant for some processes related to biofuel production.

To utilise collision cross sections in simulations, the data must adequately describe the physical processes over the complete and diverse range of kinematical conditions relevant to the process.[5,6] Unfortunately, our capability for obtaining experimental cross-sections over such a vast range of kinematics is quite limited owing to long experimental run times. This generates a pressing demand for new theoretical models that are able to accurately and efficiently compute those complete cross-section sets. The role of experiments is therefore to provide definitive tests to validate, or at least understand the limitations of, theoretical models.

In the present investigation, we utilise an (e,2e) technique to investigate the dynamics of electron impact ionisation of phenol. These experiments are compared to theoretical calculations obtained within a molecular 3-body distorted wave (M3DW) framework. Note that the M3DW approach has been demonstrated to be quite successful in reproducing collision cross section data for the low and intermediate-energy electron impact ionisation of atoms and molecules.[19] The present work extends our previous results for molecules of some biological interest, such as pyrimidine,[20] tetrahydrofuryl alcohol (THFA),[21,22] tetrahydrofuran (THF),[22,23] 1,4-dioxane,[23,24] and tetrahydropyran (THP).[24]

The structure of the present paper is as follows. In Sec. II, we discuss our experimental techniques and analysis procedures, while in Sec. III a brief description is provided in regard to the present computations. Thereafter, in Sec. IV, our results and a discussion of those results is presented, before some conclusions from the current investigation are drawn.

II. EXPERIMENTAL METHOD

We have used an (e,2e) coincidence technique, under coplanar asymmetric kinematical conditions, to obtain a selection of triple differential cross sections for electron-impact ionisation of phenol. A detailed description of the employed method can be found elsewhere.[20–24] Briefly, however, a well-collimated beam of electrons with energy $E_0 = 250$ eV collide with gaseous phenol at low pressure, with some electrons ionising the phenol target to yield two-outgoing electrons. The present high-purity sample of phenol was sourced from Ajax Unilab (assay $>$ 99%), and is a solid at room temperature. Nonetheless, it readily sublimes under vacuum. To assist in producing a stable beam of phenol, the sample was heated to a modest temperature of 40–45 °C. Phenol-vapour was then introduced into the interaction region through a needle, with the flow rate being controlled by a variable leak valve. Note that our chamber and gas handling lines were heated to slightly higher temperatures to prevent the formation of phenol deposits within the chamber.

In the present asymmetrical kinematics of our experiments, we detect a fast electron with energy E_a, commonly referred to as the scattered electron, and a slow electron with energy E_b, usually referred to as the ejected electron, although of course the electrons are actually indistinguishable. Here, the scattered and ejected electrons are detected at angles referenced to the incident beam direction, θ_a and θ_b, respectively. In our experiment, a time coincident technique is used to ensure that both electrons originated from the same ionisation event. The energy required to ionise the electron bound to phenol ϵ_i can then be determined through the conservation of energy,

$$\epsilon_i = E_0 - E_b - E_a. \quad (1)$$

Note that by keeping the incident electron and slow ejected electron energies fixed, binding energy spectra (BES) can be obtained by recording the number of true coincident events as the scattered electron energy is varied. The BES of phenol, measured with scattered and ejected electron angles of $\theta_a = -10°$ and $\theta_b = 75°$, respectively, is presented in Fig. 2. Note that the orbital assignments presented in Fig. 2 are taken from Kishimoto *et al.*,[25] and are supported by our own quantum chemistry calculations conducted as a part of this study (see later). Good qualitative agreement between the present BES, over the range of binding energies $\epsilon_i \sim 7$–16.5 eV, and the earlier He I ultraviolet photoelectron spectra (UPS) study of Kishimoto *et al.*[25] was found, although the superior energy resolution of the UPS technique ensured that more orbital-based features could be resolved. The coincidence energy resolution in the present measurements was estimated to be 1.1 eV (FWHM), while the Gaussian functions employed in our least-squares spectral deconvolution fit

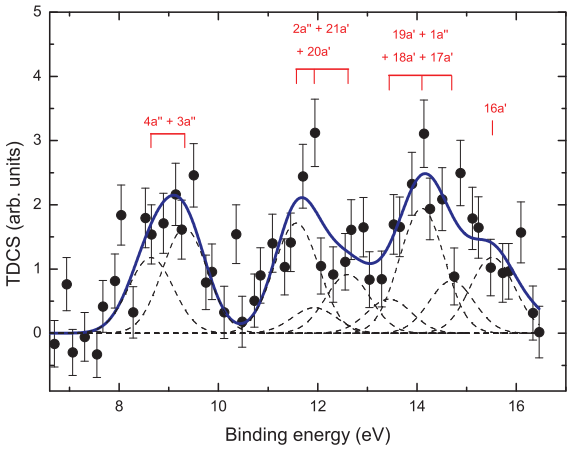

FIG. 2. Measured binding energy spectrum of phenol (•) obtained for an incident energy of 250 eV, and scattered and ejected electron detection angles of $\theta_a = -10°$ and $\theta_b = 75°$, respectively. Also shown are the spectral deconvolutions of the measured spectra into contributions from each orbital feature (– –) and their sum (—). See text for further details.

of the BES, as represented by the short-dashed curves (again see Fig. 2), possessed widths that were a convolution of the (e,2e) coincidence energy resolution and the natural widths of the various orbital manifolds, as taken from the UPS spectrum. The overall fit (solid line) to the coincidence data in our BES is seen to be very good, and clearly defines the unresolved highest-occupied molecular orbital (HOMO, 4a″) and next highest-occupied molecular orbital (NHOMO, 3a″) to be at $\epsilon_i \sim 9$ eV.

TDCS describing the angular distribution of the ejected electron $E_b = 20$ eV are obtained for the electron impact ionisation of the unresolved combination of the HOMO and NHOMO of phenol ($\epsilon_i \sim 9$ eV) when the scattered electrons were detected at fixed polar angles of $\theta_a = -5^\circ$, -10°, and -15°. For each angular position of the scattered electron analyser, the number of true coincident counts was recorded when the slow electron was detected in the angular ranges from $\theta_b = 55^\circ$ to 120°, and from $\theta_b = 240^\circ$ to 285°. Those angular ranges encompass the so-called binary and recoil peak regions, respectively. Note that the angular range of our ejected electrons is largely limited by the considerable physical dimensions of the analysers.

The kinematical conditions for this study were chosen to study ionisation dynamics at the bound Bethe-Ridge and below. The bound Bethe-Ridge is sometimes referred to as an ideal collision, where the recoil ion acts like a spectator (and so does not take any momentum). It happens exactly when the magnitude of the momentum transfer $|\boldsymbol{K}|$ is equal to that for the ejected electron $|\boldsymbol{k}_b|$. Here, the momentum transfer is defined as:

$$\boldsymbol{K} = \boldsymbol{k}_0 - \boldsymbol{k}_a, \tag{2}$$

where $\boldsymbol{k}_0$ and $\boldsymbol{k}_a$ are the incident and scattered electron momenta, respectively. When the slow electron is ejected in a direction close to that of $\boldsymbol{K}$, it absorbs most of the momentum transferred in the collision, and the collision is said to be binary. Conversely, when the slow electron is directed in the direction anti-parallel to that of the momentum transfer, the ion possess substantial momentum and the collisions are said to be recoil in nature. The relative intensity of the TDCS in the binary and recoil regions therefore contain signatures relating to the dynamics of the ionisation process.[20–24]

III. THEORY

The theoretical results were calculated using the molecular three-body distorted wave approximation, coupled with an orientation-averaged molecular orbital (OAMO) approximation, and either an approximate or exact description of the post-collision interaction (PCI).[19] The direct-scattering T-matrix integral in this formalism is given by:

$$T_{dir} = \left\langle \underbrace{\chi_a^-(\boldsymbol{k}_a, \boldsymbol{r}_1)\chi_b^-(\boldsymbol{k}_b, \boldsymbol{r}_2)C_{scat-ejec}(\boldsymbol{r}_{12})}_{Final\ state} \middle| \frac{1}{r_{12}} - U_a(r_1) \middle| \underbrace{\phi_{DY}^{OA}(\boldsymbol{r}_2)\chi_0^+(\boldsymbol{k}_0, \boldsymbol{r}_1)}_{Initial\ state} \right\rangle. \tag{3}$$

In this approach, the initial state consists of the incident distorted wave $\chi_0^+(\boldsymbol{k}_0, \boldsymbol{r}_1)$ and the orientation averaged Dyson orbital $\phi_{DY}^{OA}(\mathbf{r}_2)$. This Dyson orbital defines the overlap of the many-electron wave functions of the initial and ionised states of the system, and can be approximated by the ionised Kohn-Sham orbitals under a frozen-core approach. The molecular wave functions were calculated using density functional theory (DFT), along with the standard hybrid B3LYP functional,[26] using ADF 2007 (the Amsterdam Density Functional program[27]) with a TZ2P (triple-zeta with two polarisation functions) Slater-type basis set. These orbitals were averaged over all molecular orientations within the so-called OAMO approach.[28] The potential U_a represents the spherically symmetric interaction between the projectile and the active electron, and $\boldsymbol{r}_{12}$ is the relative distance between the outgoing electrons. The final state consists of distorted waves $\chi_a^-(\boldsymbol{k}_a, \boldsymbol{r}_1)$ and $\chi_b^-(\boldsymbol{k}_b, \boldsymbol{r}_2)$ for the outgoing electrons multiplied by $C_{scat-ejec}(\boldsymbol{r}_{12})$, that is, a factor that describes the Coulomb interaction between the ejected and scattered electrons. The Coulomb interaction between those two electrons can be expressed as a product of a gamma (Γ) function and a confluent hypergeometric function ${}_1\mathrm{F}_1$:

$$C_{scat-ejec} = e^{-\pi\gamma/2}\Gamma(1-i\gamma)\,{}_1F_1(i\gamma, 1, -i(k_{12}r_{12} + \boldsymbol{k}_{12}\cdot\boldsymbol{r}_{12})). \tag{4}$$

In Eq. (4), $\boldsymbol{k}_{12} = \mu\boldsymbol{v}_{12}$, where μ is the reduced mass for two electrons, $\boldsymbol{v}_{12}$ is the relative velocity between them, and γ is the Sommerfeld parameter ($\gamma = 1/v_{12}$) that determines the strength of the interaction.

If one uses the Coulomb interaction as presented above, a numerical 6D integral is required to evaluate the T-matrix, demanding long computational times especially for large molecules. The difficulty arises from the hypergeometric function that cannot be factored out from the integral without appropriate simplification. Some authors have suggested that the PCI might be overestimated at lower energies,[19] and that the approximation given by Ward and Macek[29] for low energies can provide accurate results. In that approximation, $\boldsymbol{r}_{12}$ is replaced by an average value that is parallel to $\boldsymbol{k}_{12}$. This simplifies the numerical calculation significantly, since the Coulomb interaction can now be factored from the T-matrix integral. Another further simplification can be made by just neglecting the hypergeometric function,[30,31] so approximating $|C_{scat-ejec}|^2$ to the Gamow factor that is defined as:

$$N_{ee} = |e^{-\pi\gamma/2}\Gamma(1 - i\gamma)|^2. \tag{5}$$

The final TDCS cross-section is calculated using the direct and exchange-scattering amplitudes as follows:

$$\frac{d\sigma}{d\Omega_a d\Omega_b dE_b} = \frac{1}{(2\pi)^5}\frac{k_a k_b}{k_0}(|T_{dir}|^2 + |T_{exc}|^2 + |T_{dir} - T_{exc}|^2), \tag{6}$$

where T_{exc} is the exchange-scattering T-matrix that is calculated similar to T_{dir}, except that the particles 1 and 2 are interchanged in the final state.

In this work, the TDCS for single electron-impact ionisation of phenol was obtained using the M3DW approach with the Coulomb interaction treated either exactly, or approximated using the Ward-Macek approximation, or approximated by neglecting the hypergeometric function which

is referred to as the Gamow approximation. In order to determine the importance of PCI, we also perform calculations, designated DWBA, that do not incorporate any post-collisional Coulomb interaction.

To assist in the interpretation of the present BES and TDCS results, quantum chemical calculations on phenol were also performed at the B3LYP/aug-cc-pVDZ level in GAUSSIAN09.[32] These calculations were employed to assist us in our orbital assignments and to derive orbital momentum profiles for the unresolved HOMO (4a″) and NHOMO (3a″) studied experimentally. Those momentum profiles were calculated using the HEMS program described in Cook and Brion.[33]

IV. RESULTS AND DISCUSSION

Figure 3 shows the present triple differential cross-section angular distributions of the ejected electron produced in the ionisation of the HOMO+NHOMO of phenol, in the three asymmetric coplanar kinematical conditions for the scattered electron angles $\theta_a = -5°, -10°$, and $-15°$. The data were taken as a function of the ejected electron angle, in the scattering plane, using $E_0 = 250$ eV and $E_b = 20$ eV. Momentum profiles for the ionised HOMO+NHOMO (π_3 and π_2) MOs are also presented in Fig. 4. In both the HOMO and the NHOMO, the ionised orbitals are dominated by out-of-plane delocalised π orbitals, specifically by C($2p$) and O($2p$)

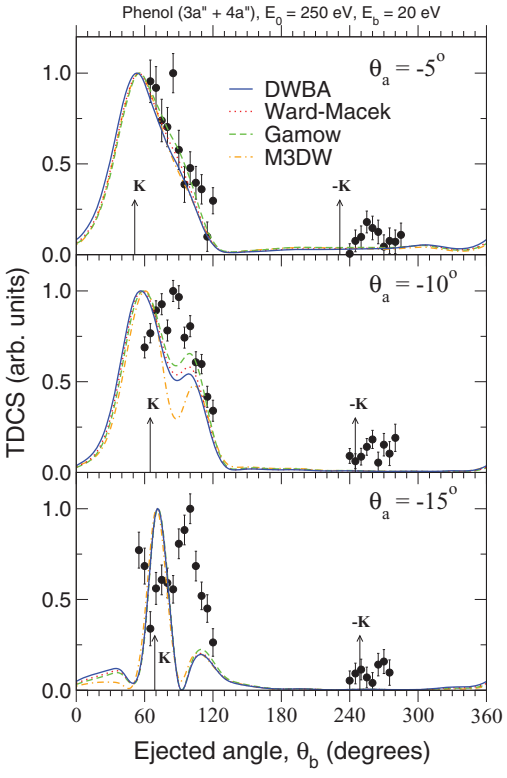

FIG. 3. TDCS for electron impact ionisation of the HOMO and NHOMO of phenol (4a″ + 3a″) with $E_0 = 250$ eV, $E_b = 20$ eV and transferred momenta of 0.45 a.u. ($\theta_a = -5°$), 0.77 a.u. ($\theta_a = -10°$), and 1.12 a.u. ($\theta_a = -15°$), respectively. The M3DW calculation results with the Coulomb interaction treated exactly (M3DW) and approximately are compared to the experimental results (•). The arrows represent the directions parallel (***K***) and anti-parallel (− ***K***) to the transferred momentum.

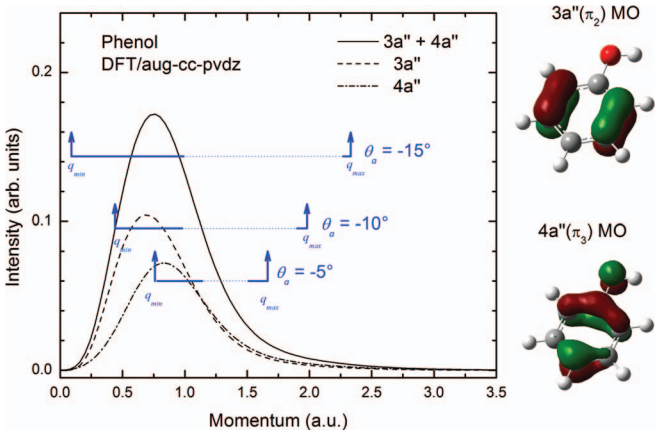

FIG. 4. Momentum profiles of the 4a″ HOMO, 3a″ NHOMO, and the sum 4a″ + 3a″ of phenol. The arrows indicate the accessible range of recoil momentum values covered in the kinematical conditions of our experiment. Also shown are diagrammatic representations of the HOMO and NHOMO orbitals. See text for further details.

electrons. The dominant "p-like" character of the ionised orbitals is clearly evident from the momentum profile, with a minimum at 0 a.u. Here, we note that under the present kinematical conditions, with intermediate to small incident and outgoing electron energies and a small momentum transferred to the target, the recoil momentum of the ion (***q***), to conserve momentum, is not equal in magnitude and opposite in sign to the target electron's momentum at the instant of ionisation (as in electron momentum spectroscopy[34]). However, the momentum profiles should still provide clues to the observed experimental behaviour. For this purpose, in Fig. 4, we also show arrows that detail the region of recoil momentum covered, when the fast electron is detected at the specific scattering angles covered in our experiments.

The present experiments are obtained in a relative fashion, owing to the complexity and long experimental runtimes required to inter-normalize or place on an absolute scale.[35] We are therefore limited to assessing the angular distribution of the slow ejected electron for each scattering angle. From the theoretical perspective, the inclusion of different PCI models influences the absolute magnitude of the result. Thus, in order to assess the shapes of each calculation in reproducing the experimental data, we normalize all experimental and theoretical results to unity at a single point. The absolute numbers from our calculations are available on request.

Fig. 3 shows a varying level of agreement between the experimental data and the cross-section calculations. These variations are strongly dependant on the kinematical condition in question. We begin by discussing the behaviour observed in the binary region. For $\theta_a = -5°$, we observe excellent agreement in terms of the shape between the distorted wave calculations and the experimental measurement. This result is somewhat surprising in that previously the distorted wave calculations have failed to reproduce the experimental width of the binary feature of other molecular targets[20–24] under this same kinematical condition. However, when we consider the binary regions for the other kinematical conditions of $\theta_a = -10°$ or $-15°$, we see substantial differences between the experimental data and the distorted wave calculations.

Here, we note that all our theoretical calculations are largely consistent with one another, which suggests we rule out PCI effects as the origin of the observed discrepancies. The angular distribution for $\theta_a = -15^\circ$ displays a deep minimum in the vicinity of the momentum transfer direction. This minimum is characteristic of the strong *p*-like character of the ionised orbital. Interestingly, the distorted wave calculations give maxima in the vicinity of the momentum transfer for both $\theta_a = -10^\circ$ and -15°. This behaviour was noted in our previous investigations, however it was somewhat mitigated by the *s*-type or *sp*-hybrid nature of the orbitals ionised in those investigations. For phenol, where the HOMO+NHOMO is dominated by out-of-plane atomic 2*p* contributions, the failure of the orientation averaging approach becomes inherently obvious for the $\theta_a = -10^\circ$ and -15° conditions. Indeed, we note that the orientation averaging approach is known to be problematic for the asymmetric *p*-like orbital contributions.[36] In a recent publication by Chaluvadi *et al.*,[37] the OAMO approximation was replaced by a proper average over orientation dependent cross sections and much better agreement with experiment was found for methane. Trial calculations have indicated that there is a high probability that, for *p*-type states, the proper average method will produce a split binary peak similar to that observed in the experimental data. Unfortunately, these proper average calculations are so computationally expensive that they can only run on very large computing clusters, such as the US Extreme Science and Engineering Discovery Environment (XSEDE). We currently have a pending proposal requesting time on the XSEDE clusters to calculate proper average cross sections for some of these large molecules that have been measured at Flinders.[20–24] Overall, the effects of PCI are quite small with the largest difference found for $\theta_a = -10^\circ$. Interestingly, for all three measured cases, the Gamow approximation gives results that are slightly closer to experiment than the other two treatments.

Now we turn our attention to the recoil region. Here, the calculated TDCS underestimates the strength of the measured TDCS in the recoil region for all conditions. This observation is consistent with previous studies employing the same theoretical approach for other molecular targets,[20–24] where the calculation persistently underestimates the strength of the TDCS in the recoil region. However, this observation is somewhat tempered for the HOMO+NHOMO of phenol by the absence of any significant recoil peak intensity across the range of kinematical conditions studied. We do, however, note that at $\theta_a = -5^\circ$, there is experimental evidence of a peak centred on $\theta_b \sim 260^\circ$ (see Fig. 3). Here, all theoretical methods support the existence of a recoil feature, as all of the methods give rise to a small peak centred in the vicinity of $\theta_b \sim 300^\circ$. The absence of any substantial experimental recoil peak intensity is particularly notable for the phenol target. In our earlier investigations on other molecular targets, conducted under similar kinematical conditions, prominent recoil peak intensities have been observed (especially for $\theta_a = -5^\circ$). Previously, Xu *et al.*[38] have commented that the strength of the recoil peak intensity could be related to the orbital momentum profile. In that work, they stated that the *p*-like profile, having a reduced binary maximum, may exhibit a larger recoil peak, relatively speaking. Based on these assumptions, one may therefore expect significant recoil peak intensity for the unresolved HOMO and NHOMO of phenol, being dominated by *p*-type orbital contributions. However, this is clearly not the case. One possible explanation for this behaviour is the nature of the ionised orbital. In this case, we note that the HOMO+NHOMO of phenol are both diffuse π-bonding orbitals. This differs significantly from the orbitals of THF, THFA, THP, and 1,4-dioxane studied in our earlier investigations,[20–24] where the ionised orbitals were dominated by O(2*p*) lone electron pairs that are centralised on the oxygen atom, which then couple to the carbon σ-frame. In phenol, the delocalisation of the orbital over the entire molecule may reduce electron-interactions with the nuclei that are classically required for recoil scattering. However, this notion requires detailed theoretical investigation before definitive conclusions can be deduced. From the theoretical perspective, the absence of recoil intensity in the M3DW framework may be explained by the absence of nuclear charge at the centre of mass. Here, the nuclear charge is re-distributed over spherical shells that are known to reduce the distortion experienced by the outgoing electron.[39]

The present investigation, together with our earlier studies, suggest that the dynamics of the ionisation process is governed by a multitude of factors, relating to both the nature of the ionised orbital and how that orbital interacts with localised nuclei. Indeed, computationally demanding proper-averaged calculations[37] may be required to shed further light into these issues.

V. CONCLUSIONS

We have presented experimental and theoretical TDCS results for phenol. The approach used in the theoretical calculations of the TDCS was the M3DW, coupled with an orientation-averaged molecular orbital approximation, and with PCI treated either exactly or approximately. The TDCS data for the electron-impact ionisation of phenol were obtained under coplanar asymmetrical kinematics with incident energy of 250 eV. Here, the kinematical configurations were chosen to correspond to the region near the bound Bethe-Ridge. The experimental data were taken on the 4a″ and 3a″ orbitals, that unfortunately could not be resolved, given our coincidence energy resolution. The level of agreement between the calculations and experimental data was strongly dependent on the kinematical configurations investigated in this work, being much better at smaller momentum transfer. The theoretical calculations further suggest that PCI is not necessarily playing an important role under these kinematical conditions and may be neglected in the first instance. The more important approximation is the OAMO and we expect that the properly averaged cross sections will be in better accord with experiment. We will perform the proper average cross sections as soon as we can obtain the necessary computational resources.

ACKNOWLEDGMENTS

This research was supported by the Australian Research Council (ARC) Centre of Excellence for Antimatter-Matter

Studies, by the U.S. National Science Foundation (NSF) under Grant. No. PHY-1068237 (E.A. and D.H.M.), and by the National Natural Science Foundation of China (NNSFC) under Grant No. 11174175 (C.G.N.). G.B.S. thanks the Brazilian government through CAPES (Proc. No. BEX 17756/12-0) and Flinders University for financial assistance during his stay in Australia. D.B.J. gratefully acknowledges support provided through an ARC Discovery Early Career Researcher Award. R.F.C.N. also acknowledges CNPq for financial support that enabled him to study in Australia. M.C.A.L. acknowledges financial support from CNPq. Finally, M.J.B. acknowledges CNPq for his "Special Visiting Professor" appointment.

[1]L. G. Christophorou and J. K. Olthoff, *Fundamental Electron Interactions with Plasma Processing Gases* (Kluwer Academic, New York, 2004).
[2]L. Campbell and M. J. Brunger, Plasma Sources Sci. Technol. **22**, 013002 (2013).
[3]B. Boudaiffa, P. Cloutier, D. Hunting, M. A. Huels, and L. Sanche, Science **287**, 1658 (2000).
[4]I. Bray, D. Fursa, A. Kadyrov, A. Stelbovics, A. Kheifets, and A. Mukhamedzhanov, Phys. Rep. **520**, 135 (2012).
[5]A. G. Sanz, M. C. Fuss, A. Muñoz, F. Blanco, P. Limão-Vieira, M. J. Brunger, S. J. Buckman, and G. García, Int. J. Radiat. Biol. **88**, 71 (2012).
[6]R. D. White, W. Tattersall, G. Boyle, R. E. Robson, S. Dujko, Z. Lj. Petrovic, A. Bankovic, M. J. Brunger, J. P. Sullivan, S. J. Buckman, and G. Garcia, Appl. Radiat. Isot. **83**, 77 (2014).
[7]L. Sanche, Eur. Phys. J. D **35**, 367 (2005).
[8]H. Nikjoo, P. O'Neill, M. Terrissol, and D. Goodhead, Radiat. Environ. Biophys. **38**, 31 (1999).
[9]N. Schultz-Jensen, Z. Kádár, A. B. Thomsen, H. Bindslev, and F. Leipold, Appl. Biochem. Biotechnol. **165**, 1010 (2011).
[10]L. Klarhöfer, W. Viöl, and W. Maus-Friedrichs, Holzforschung **64**, 331 (2010).
[11]J. A. Souza-Corrêa, M. A. Ridenti, C. Oliveira, S. R. Araújo, and J. Amorim, J. Phys. Chem. B **117**, 3110 (2013).
[12]J. Amorim, C. Oliveira, J. A. Souza-Corrêa, and M. A. Ridenti, Plasma Process. Polym. **10**, 670 (2013).
[13]A. J. Ragauskas, C. K. Williams, B. H. Davison, G. Britovsek, J. Cairney, C. A. Eckert, W. J. Frederick, J. P. Hallett, D. J. Leak, C. L. Liotta, J. R. Mielenz, R. Murphy, R. Templer, and T. Tschaplinski, Science **311**, 484 (2006).
[14]M. E. Himmel, S.-Y. Ding, D. K. Johnson, W. S. Adney, M. R. Nimlos, J. W. Brady, and T. D. Foust, Science **315**, 804 (2007).
[15]M. N. R. Ashfold, B. Cronin, A. L. Devine, R. N. Dixon, and M. G. D. Nix, Science **312**, 1637 (2006).
[16]O. P. J. Vieuxmaire, Z. Lan, A. L. Sobolewski, and W. Domcke, J. Chem. Phys. **129**, 224307 (2008).
[17]E. M. de Oliveira, S. d'A. Sanchez, M. H. F. Bettega, A. P. P. Natalense, M. A. P. Lima, and M. T. do N. Varella, Phys. Rev. A **86**, 020701(R) (2012).
[18]D. B. Jones, G. B. da Silva, R. F. C. Neves, H. V. Duque, L. Chiari, E. M. de Oliveira, M. C. A. Lopes, R. F. da Costa, M. T. do N. Varella, M. H. F. Bettega, M. A. P. Lima, and M. J. Brunger, J. Chem. Phys. **141**, 074314 (2014).
[19]D. H. Madison and O. Al-Hagan, J. At. Mol. Opt. Phys. **2010**, 367180 (2010).
[20]J. Builth-Williams, S. M. Bellm, D. B. Jones, H. Chaluvadi, D. Madison, C. G. Ning, B. Lohmann, and M. J. Brunger, J. Chem. Phys. **136**, 024304 (2012).
[21]S. M. Bellm, J. D. Builth-Williams, D. B. Jones, H. Chaluvadi, D. H. Madison, C. G. Ning, F. Wang, X. G. Ma, B. Lohmann, and M. J. Brunger, J. Chem. Phys. **136**, 244301 (2012).
[22]D. B. Jones, J. D. Builth-Williams, S. M. Bellm, L. Chiari, H. Chaluvadi, D. H. Madison, C. G. Ning, B. Lohmann, O. Ingólfsson, and M. J. Brunger, Chem. Phys. Lett. **572**, 32 (2013).
[23]J. D. Builth-Williams, S. M. Bellm, L. Chiari, P. A. Thorn, D. B. Jones, H. Chaluvadi, D. H. Madison, C. G. Ning, B. Lohmann, G. B. da Silva, and M. J. Brunger, J. Chem. Phys. **139**, 034306 (2013).
[24]J. D. Builth-Williams, G. B. da Silva, L. Chiari, D. B. Jones, H. Chaluvadi, D. H. Madison, and M. J. Brunger, J. Chem. Phys. **140**, 214312 (2014).
[25]N. Kishimoto, M. Furuhashi, and K. Ohno, J. Electron Spectrosc. Relat. Phenom. **113**, 35 (2000).
[26]C. Lee, W. Yang, and R. G. Parr, Phys. Rev. B **37**, 785 (1988).
[27]G. te Velde, E. Baerends, C. Fonseca Guerra, S. van Gisbergen, J. Snijders, and T. Ziegler, J. Comput. Chem. **22**, 931 (2001).
[28]J. F. Gao, D. H. Madison, and J. L. Peacher, J. Chem. Phys. **123**, 204314 (2005).
[29]S. J. Ward and J. H. Macek, Phys. Rev. A **49**, 1049 (1994).
[30]J. Botero and J. H. Macek, Phys. Rev. Lett. **68**, 576 (1992).
[31]C. T. Whelan, R. J. Allan, and H. R. Walters, J. Phys. IV France **3**(C6), 39 (1993).
[32]M. J. Frisch, G. W. Trucks, H. B. Schlegel *et al.*, Gaussian 09, Revision B.01 Gaussian, Inc., Wallington, CT, 2010.
[33]J. P. Cook and C. Brion, Chem. Phys. **69**, 339 (1982).
[34]E. Weigold and I. McCarthy, *Electron Momentum Spectroscopy* (Kluwer Academic, New York, 1999).
[35]L. R. Hargreaves, M. A. Stevenson, and B. Lohmann, Meas. Sci. Technol. **21**, 055112 (2010).
[36]J. F. Gao, J. L. Peacher, and D. H. Madison, J. Chem. Phys. **123**, 204302 (2005).
[37]H. Chaluvadi, C. G. Ning, and D. Madison, Phys. Rev. A **89**, 062712 (2014).
[38]S. Xu, X. Ma, S. Yan, and P. Zhang, J. Chem. Phys. **136**, 237101 (2012).
[39]I. Tóth and L. Nagy, J. Phys. B **43**, 135204 (2010).